Online Supplement

Autophagy In Mesenchymal Progenitors Protects Mice Against Bone Marrow Failure After Severe Intermittent Stress

Theresa Landspersky[1], Mehmet Saçma[2], Jennifer Rivière[1], Judith S. Hecker[1], Franziska Hettler[1], Erik Hameister[3], Katharina Brandstetter[4], Rouzanna Istvánffy[1,5], Sandra Romero Marquez[1], Romina Ludwig[1], Marilena Götz[1], Michèle Buck[1], Martin Wolf[6], Matthias Schiemann[7], Jürgen Ruland[3], Dirk Strunk[6], Akiko Shimamura[9], Kasiani Myers[10], Terry P. Yamaguchi[11], Matthias Kieslinger[12], Heinrich Leonhardt[4], Florian Bassermann[1,8], Katharina S. Götze[1,8], Hartmut Geiger[2], Christina Schreck[1,13], Robert A.J. Oostendorp[1,13]

Affiliations

1. Technical University of Munich. School of Medicine. Clinic and Polyclinic for Internal Medicine III. Laboratory of Stem Cell Physiology, 81675 Munich, Germany
2. Institute of Molecular Medicine, Ulm University, 89081 Ulm, Germany.
3. Technical University of Munich. School of Medicine. Clinical Chemistry and Pathobiochemistry, 81675 Munich, Germany
4. Human Biology and BioImaging, Faculty of Biology, Ludwig-Maximilians-Universität München, 81377 Munich, Germany.
5. Current address: Technical University of Munich, Klinikum rechts der Isar, Department of Surgery, 81675 Munich, Germany
6. Institute of Experimental and Clinical Cell Therapy, Paracelsus University Salzburg, 5020 Salzburg, Austria
7. Technical University of Munich (TUM), Institute for Medical Microbiology, Immunology and Hygiene, CyTUM-MIH , 81675 Munich, Germany
8. German Cancer Consortium (DKTK), 69120 Heidelberg, Germany
9. Bone Marrow Failure and MDS Program, Dana Farber and Boston Children's Hospital, Boston, MA 02115, USA
10. Division of Bone Marrow Transplantation and Immune Deficiency, Cincinnati Children's Hospital Medical Center, Cincinnati, OH, USA
11. Cancer and Developmental Biology Laboratory, Center for Cancer Research, National Cancer Institute-Frederick, NIH, Frederick, MD 21702, USA.
12. Department for Small Animals and Horses, University of Veterinary Medicine, 1210 Vienna, Austria

Methods to the supplementary Figures

Colony-forming unit fibroblast (CFU-F) assay

Fibroblastic colony-forming units (CFU-F) were assessed from sorted primary MSPCs (100 cells/cm^2) or cultured MSPCs (300 cells/cm^2). For this, MSPCs were plated on 0,1% gelatine-coated well plates in MEM Alpha (with Ribosides and Glutamax, Life Technologies), supplemented with 10% Fetal Calf Serum (FCS, PAA), antibiotics, and 0,1% β-Mercapto-ethanol (Invitrogen). Adherent fibroblast-like colonies were microscopically enumerated after four days (cultured MSPCs) or two weeks (primary sorted MSPCs).

Long-term culture of MSPCs

For determination of growth curves, MSPCs were cultured for at least 8 passages. Growing cells were passaged at approximately 70% confluence and reseeded at a density of 1x10^3 cells/cm^2. Cumulative population doublings (PD) were calculated from the number of cells seeded and the number of cells harvested at the next passage as described previously [1].

Differentiation assay

Adipogenic and osteogenic potential of MSPCs was determined using commercially available differentiation media as described by the manufacturer (StemXVivo®; R&D Systems). For staining, cells were rinsed with PBS and fixed in 10% paraformaldehyde (PFA) for 15 min at RT. Adipogenic potential was determined by staining with Oil Red O and visual examination and quantitation using propanol-extracted dye and measurement at 520 nm. Osteogenic potential was determined by Alizarin Red S staining with visual

examination and quantitation using destaining solution (10% Cetylpyridiumchloride in 10 mM Sodiumphosphate (pH 7.0))-eluted dye measurement at 562 nm.

Cytomorphology

BM smears were stained with May Grunwald and Giemsa staining.

Treatment with pharmacological compounds and rWNT5A.

In vitro: to inhibit CDC42 activation, we used the CDC42/RhoGDI inhibitor CASIN (8-Cyclopentyl-2,3,3a,4,5,6-hexahydro-1H-pyrazino[3,2,1-jk]carbazole; TOCRIS) as described in Liu et al. [2]. We also used the GTP-competitive CDC42-GTP inhibitor ML-141 ((4-[3-(4-methoxyphenyl)-5-phenyl-3,4-dihydropyrazol-2-yl] benzenesulfon-amide; TOCRIS)).

MSPCs were treated with inhibitors at 5μM or 0.01% DMSO for 4 hrs. Subsequently, cells were fixed with 4% paraformaldehyde (PFA) for 5 min for immunofluorescence (IF) staining. For autophagy measurements, WT MSPCs were treated with rapamycin (1μM), chloroquine (10μM), CASIN (5μM), or DMSO for 16 hrs.

In some experiments, MSPCs were treated with recombinant murine WNT5A (rWNT5A), a low dose of 100 ng/ml rWNT5A (R&D Systems) was added to MSPCs at 2 consecutive days, 24 hrs apart.

In vitro treatment with stress inducers

To show MSPC responses to different types of stress, compact bone-derived MSPCs (P4) were spotted on chamber slides and treated with poly(I:C) (100µM, Apexbio) for 4 h or with 5-FU (15µM, Ribosepharm) for 16 hrs. For the irradiation experiment, the cells were irradiated with 15 Gy (gamma-irradiation). Cells were fixed and analyzed by IF microscopy as described below.

AnnexinV staining

Apoptosis in compact bone-derived MSPCs was determined using AnnexinV staining in combination with propidium iodide (PI). For this purpose, cells were suspended in AnnexinV binding buffer (14 mM NaCl, 10 µM Hepes and 2.5 mM CaCl2) plus AnnexinV-FITC (eBioscience) and PI (1µg/ml) and incubated for 15 min at 4°C. Additionally, cells were stained with CD31, CD166/Alcam and SCA-1 antibodies (Supplementary Table 3). Staining of cells were analyzed by flow cytometry on a CyAn ADP LxP8.

Analysis of immunofluorescent labeled cells

To determine *total protein content*, the number of pixels per cell was assessed using ImageJ software (v1.52). Pictures within one experiment were taken under standardized conditions (light intensity, exposure, diaphragm).

To determine *stress fiber formation,* each field was counted for 1) the total number of cells; 2) the number of cells that display stress fibers and 3) the number of cells that showed weaker formation (intermediate) or no formation.

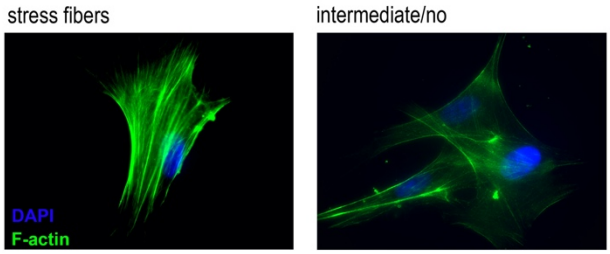

The figure below shows MSPCs with stress fiber formation (left) and intermediate /no (right).

For *mean fluorescence intensity*, the average intensity of pixels per cell was determined.

For *foci analysis,* the contrasts were visible by black and white processing within the digital images (Affinity Photo, Serif Europe Ltd). After threshold setting, cell structures were selected and counted automatically using ImageJ software.

For *diameter analysis*, contrasts were visualized using relief filters (Adobe Photoshop, Version 21.1.1). After threshold setting, cell structures were selected and length was determined using ImageJ software.

Colocalization was assessed using ImageJ after picture processing by selection of single cells, background subtraction with the rolling ball algorithm, and threshold adjustment by the autothresholding method “Moment”. The ImageJ “Colocalization" plugin was then used to recover the overlapping pixels of two analysed proteins. The pixel area occupied were then collected by using the “Analyse particles” function. To identify colocalization bias either in nuclear proximity or the cytoplasm, the DAPI signal was used to delimit the nuclear area and the nuclear and cytoplasmic fractions were reported separately.

Supplementary Figures

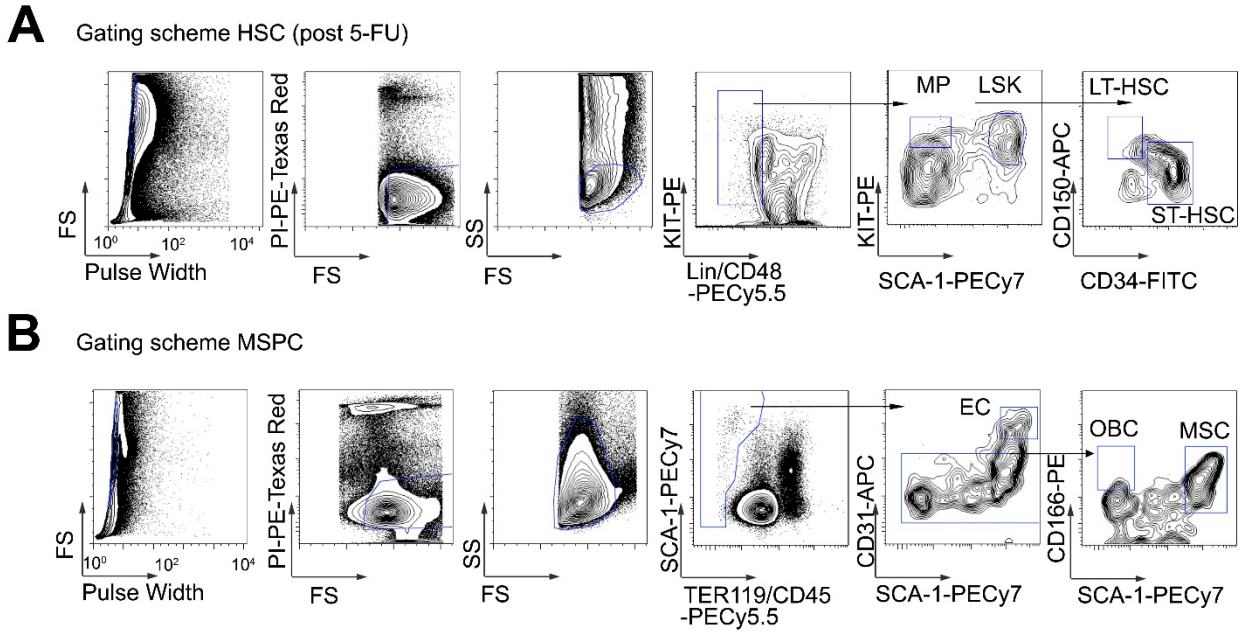

Figure S1. Gating strategies for HSCs and MSPCs flow cytometry and sorting. A, *Representative gating strategy for HSCs after 5-FU treatment. Left graph: cells were gated for Pulse Width to avoid cell doublings and to remove cell clumps. The second graph (from left) shows the viability gate to eliminate dead cells (PI^+ cells). The third gate (from left) is used to identify cells based on size (FS) and granularity (SS). Lineage$^-$ CD48$^-$ cells were gated in the fourth graph (from left). In the fifth gate (from left) MPs (Lineage$^-$ SCA-1$^-$ KIT$^+$) and LSKs (Lineage$^-$ SCA-1$^+$ KIT$^+$) cells were separated. The right graph shows LT-HSCs (CD34$^-$ CD150$^+$ CD48$^-$ LSK cells) and ST-HSCs (CD34$^+$ CD150^{low} CD48$^-$ LSK cells).* ***B,*** *Representative gating strategy for stromal subpopulations. Cells were separated due to cell doublings, viability, size and granularity (graph 1-3 from left). Next, non-hematopoietic (CD45$^-$ TER119$^-$) cells were further gated as ECs (CD31$^+$ SCA-1$^+$), MSPCs (CD31$^-$ SCA-1$^+$ Alcam$^{-/low}$) and OBCs (CD31$^-$ SCA-1$^-$ Alcam$^+$).*

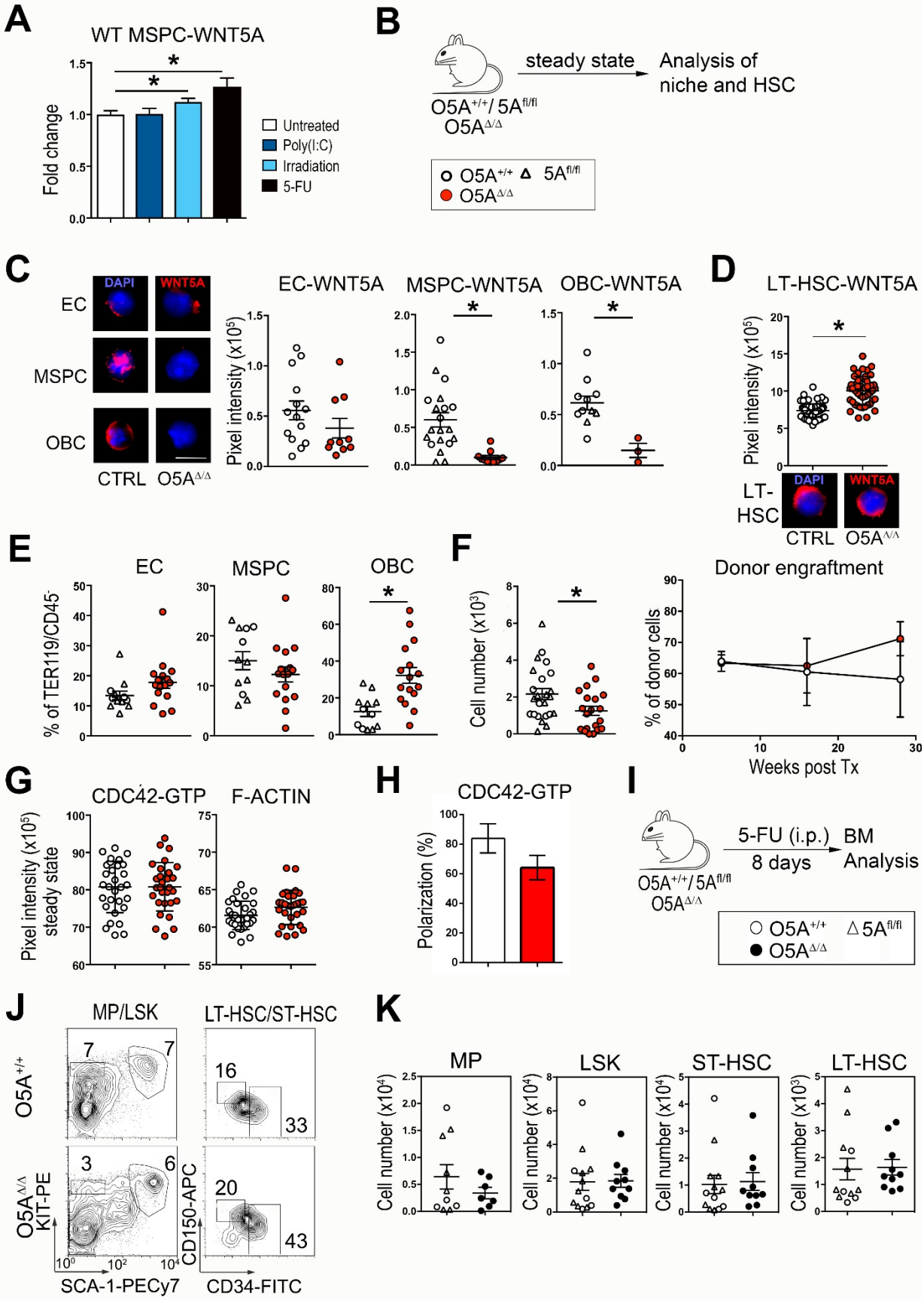
A
WT MSPC-WNT5A
Fold change
Untreated
Poly(I:C)
Irradiation
5-FU
B
steady state
Analysis of niche and HSC
O5A+/+/ 5Afl/fl
O5AΔ/Δ
O5A+/+ 5Afl/fl
O5AΔ/Δ
C
DAPI
WNT5A
EC
MSPC
OBC
CTRL O5AΔ/Δ
EC-WNT5A
MSPC-WNT5A
OBC-WNT5A
Pixel intensity (x10⁵)
D
LT-HSC-WNT5A
Pixel intensity (x10⁵)
LT-HSC
CTRL O5AΔ/Δ
E
EC
MSPC
OBC
% of TER119/CD45-
F
Cell number (x10³)
Donor engraftment
% of donor cells
Weeks post Tx
G
CDC42-GTP
F-ACTIN
Pixel intensity (x10⁵) steady state
H
CDC42-GTP
Polarization (%)
I
5-FU (i.p.)
8 days
BM Analysis
O5A+/+/ 5Afl/fl
O5AΔ/Δ
O5A+/+ 5Afl/fl
O5AΔ/Δ
J
MP/LSK
LT-HSC/ST-HSC
O5A+/+
O5AΔ/Δ
KIT-PE
SCA-1-PECy7
CD150-APC
CD34-FITC
K
MP
LSK
ST-HSC
LT-HSC
Cell number (x10⁴)
Cell number (x10³)

Figure S2. Niche cells and hematopoiesis in control and O5A$^{\Delta/\Delta}$ mice. A, *Graph shows fold change of untreated and treated WT MSPCs stained for WNT5A in IF assay. MSPCs (P4) were treated with poly(I:C), irradiated (15 Gy) or 5-FU. Pixel intensity measured by ImageJ software.* ***B,*** *Dissection of mice with the following genotypes: Control (CTRL): O5A$^{+/+}$ n=11, 5A$^{fl/fl}$ n=13 and O5A$^{\Delta/\Delta}$ n=18. Analysis of niche populations and HSCs.* ***C,*** *Fluorescent microscopy images of WNT5A (red) and DAPI (blue) staining in sorted endothelial cells (CD31$^+$ ECs) (left), mesenchymal stromal cells (CD31$^-$, Alcam^{med}/SCA-1$^+$) (middle) and osteoblastic cells (CD31$^-$, Alcam$^+$/ SCA-1$^-$OBCs) (right).* ***D,*** *Graph showing the pixel intensity of WNT5A expression in sorted LT-HSCs, measured by ImageJ software. Fluorescent microscopy images of WNT5A (red) and DAPI (blue) staining in sorted LT-HSCs.* ***E,*** *Percentage of ECs, MSPCs and OBCs; Flow cytometry gating strategy in Figure S1.* ***F,*** *Graph showing the cell numbers of LT-HSCs during steady state analysis. Primary transplantation (Tx) of 300 sorted LT-HSCs from 8-10 weeks old mice into lethally irradiated 129*Ly5.1 WT recipients. Experimental groups: O5A$^{\Delta/\Delta}$, n=3. CTRL: O5A$^{+/+}$ n=4 and 5A$^{fl/fl}$ n=2. Graph showing the donor engraftment in PB.* ***G,*** *Graphs showing the pixel intensity of CDC42-GTP and F-Actin expression in sorted LT-HSCs, measured by ImageJ software.* ***H,*** *Percentage of all sorted LT-HSCs with polar distribution of CDC42-GTP (n=30, two independent experiments), measured by ImageJ software.* ***I,*** *Experimental design for intraperitoneal (i.p.) injection of 5-FU in mice with the following genotypes: CTRL: O5A$^{+/+}$, n=5, 5A$^{fl/fl}$, n=7 and O5A$^{\Delta/\Delta}$, n=10. Analysis of LT-HSCs 8 days after treatment.* ***J****, Representative FACS plots of the BM.* ***K,*** *Graphs showing the absolute numbers of multipotent progenitors (Lin/CD48$^-$, KIT$^+$, SCA-1$^-$, MPs/left), LSKs (Lin/CD48$^-$, KIT$^+$, SCA-1$^+$/ middle left), short-term HSCs (Lin/CD48$^-$, KIT$^+$, SCA-1$^+$, CD34$^+$, CD150$^-$, ST-HSCs/middle right) and long-term HSCs (CD34$^-$, CD150$^+$ (LT-HSCs/right). Scale bars, 5µm * p-value < 0.05 (Non parametric Mann-Whitney test: A, C-H). The steady state and 5-FU analysis represent three independent experiments. Data are represented as mean ± SEM. The Tx experiment was performed once. Symbol legends in S2A, S2B and S2I.*

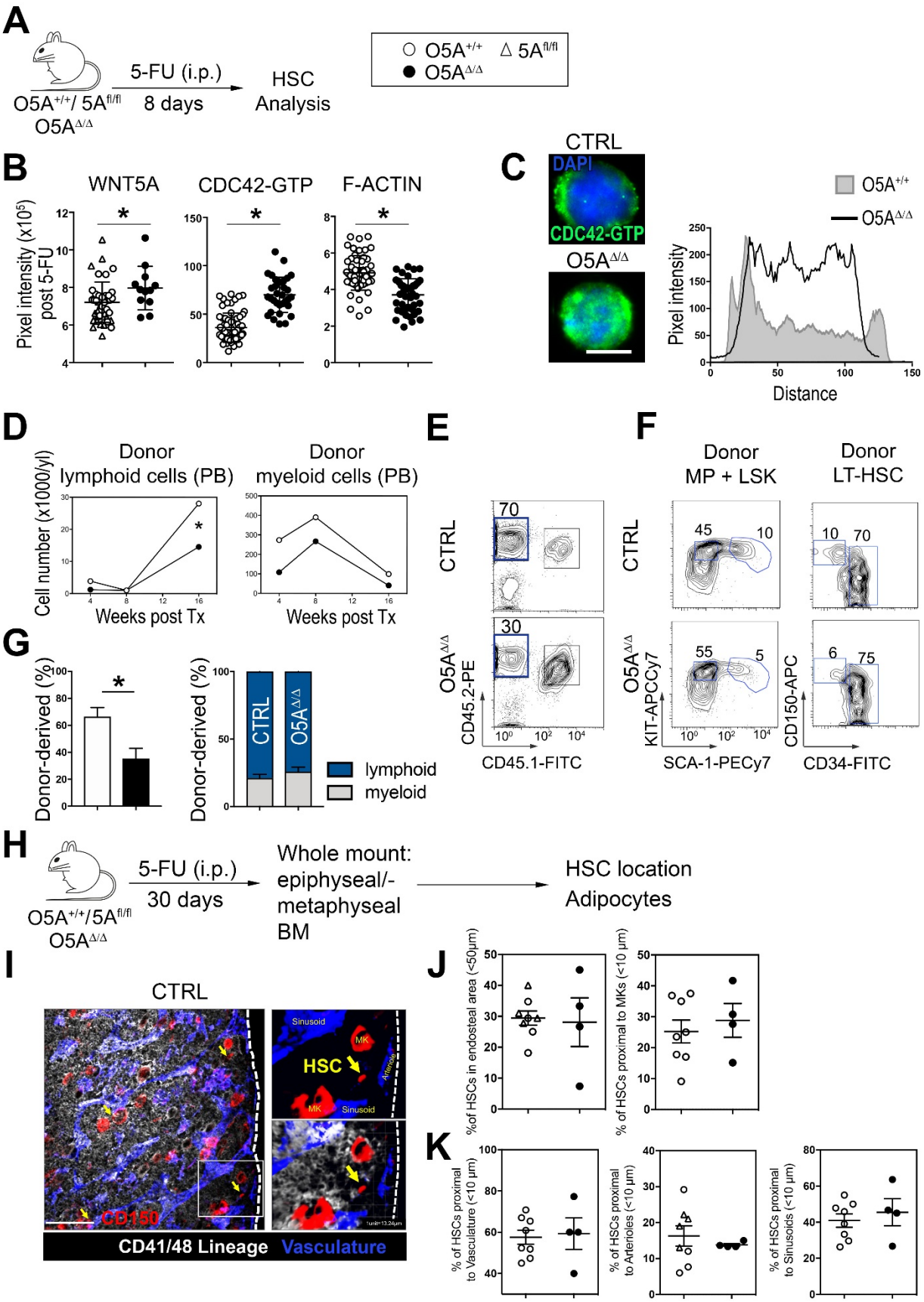
A
O5A+/+/ 5Afl/fl
O5AΔ/Δ
5-FU (i.p.)
8 days
HSC Analysis
O5A+/+ Δ 5Afl/fl
O5AΔ/Δ
B
WNT5A
CDC42-GTP
F-ACTIN
Pixel intensity (x10⁵) post 5-FU
C
CTRL
DAPI
CDC42-GTP
O5AΔ/Δ
O5A+/+
O5AΔ/Δ
Pixel intensity
Distance
D
Donor lymphoid cells (PB)
Donor myeloid cells (PB)
Cell number (x1000/µl)
Weeks post Tx
E
CTRL
O5AΔ/Δ
CD45.2-PE
CD45.1-FITC
F
Donor MP + LSK
Donor LT-HSC
KIT-APCCy7
SCA-1-PECy7
CD150-APC
CD34-FITC
G
Donor-derived (%)
lymphoid
myeloid
H
O5A+/+/5Afl/fl
O5AΔ/Δ
5-FU (i.p.)
30 days
Whole mount: epiphyseal/-metaphyseal BM
HSC location
Adipocytes
I
CTRL
Sinusoid
MK
HSC
Arteriole
CD150
CD41/48 Lineage
Vasculature
J
%of HSCs in endosteal area (<50µm)
% of HSCs proximal to MKs (<10 µm)
K
% of HSCs proximal to Vasculature (<10 µm)
% of HSCs proximal to Arterioles (<10 µm)
% of HSCs proximal to Sinusoids (<10 µm)

Figure S3. HSC and niche cell analysis of 5-FU-treated O5A$^{\Delta/\Delta}$ mice. Related to Figure 1. A, *Experimental design for intraperitoneal (i.p.) injection of 5-FU in mice with the following genotypes: Control (CTRL): O5A$^{+/+}$, n=5, 5A$^{fl/fl}$, n=7 and O5A$^{\Delta/\Delta}$, n=10. Analysis of HSCs 8 days after treatment.* ***B,*** *Graphs showing the pixel intensity of WNT5A, CDC42-GTP and F-Actin expression in sorted LT-HSCs post 5-FU treatment measured by ImageJ software.* ***C****, Representative immunofluorescence pictures of CDC42-GTP in LT-HSCs and graph showing protein distribution within the cell.* ***D,*** *Transplantation (Tx) of 300 sorted LT-HSCs 8 days after 5-FU injection into lethally irradiated 129*Ly5.1 WT recipients. Experimental groups: O5A$^{\Delta/\Delta}$, n=7. CTRL: O5A$^{+/+}$, n=5 and 5A$^{fl/fl}$, n=4. Graphs showing the absolute numbers of donor lymphoid cells (left) and donor myeloid cells (right) in peripheral blood (PB) at different time points.* ***E,*** *Representative FACS plots for CD45.2 donor cell engraftment in BM.* ***F****, Representative FACS plots for donor MPs/LSKs (left panels), and LT-HSCs (right panels).* ***G,*** *Graphs showing summary of bone marrow (BM) engraftment (left panel) and relative contribution of mature myeloid and lymphoid cells to the engrafted populations (right).* ***H,*** *Experimental design for histological evaluation of BM niche cells (see also Figure 1). I.p. injection of 5-FU in mice with the following genotypes: CTRL: O5A$^{+/+}$ n=2, 5A$^{fl/fl}$ n=2 and O5A$^{\Delta/\Delta}$ n=2. BM analysis 30 days after treatment.* ***I****, Stacked whole-mount images from epiphyseal/metaphyseal BM. FABP4^{+} vasculature is shown in blue. CD150 is shown in red, other hematopoietic markers (CD41, CD48 and lineage) are in grey. The dashed lines denote the endosteum. Zoom-out: Stacked whole-mount BM image. Zoom-in: 3D reconstructions. Scale Bar: 100µm.* ***J,*** *Graphs showing the percentage of HSCs in endosteal area (n=455 HSCs), proximal to megakaryocytes (MKs) (n=583 HSCs),* ***K,*** *proximal to vasculature/to arterioles/to sinusoids (n=610 HSCs). Analyzed from 2 mice each group, femora. Scale bars, 5µm * p-value < 0.05 (Two-sided parametric student's t test: B, D, G, J and K). Data are represented as mean ± SEM. The analysis represents the results of two independent experiments. Symbol legend shown in Figure S3A.*

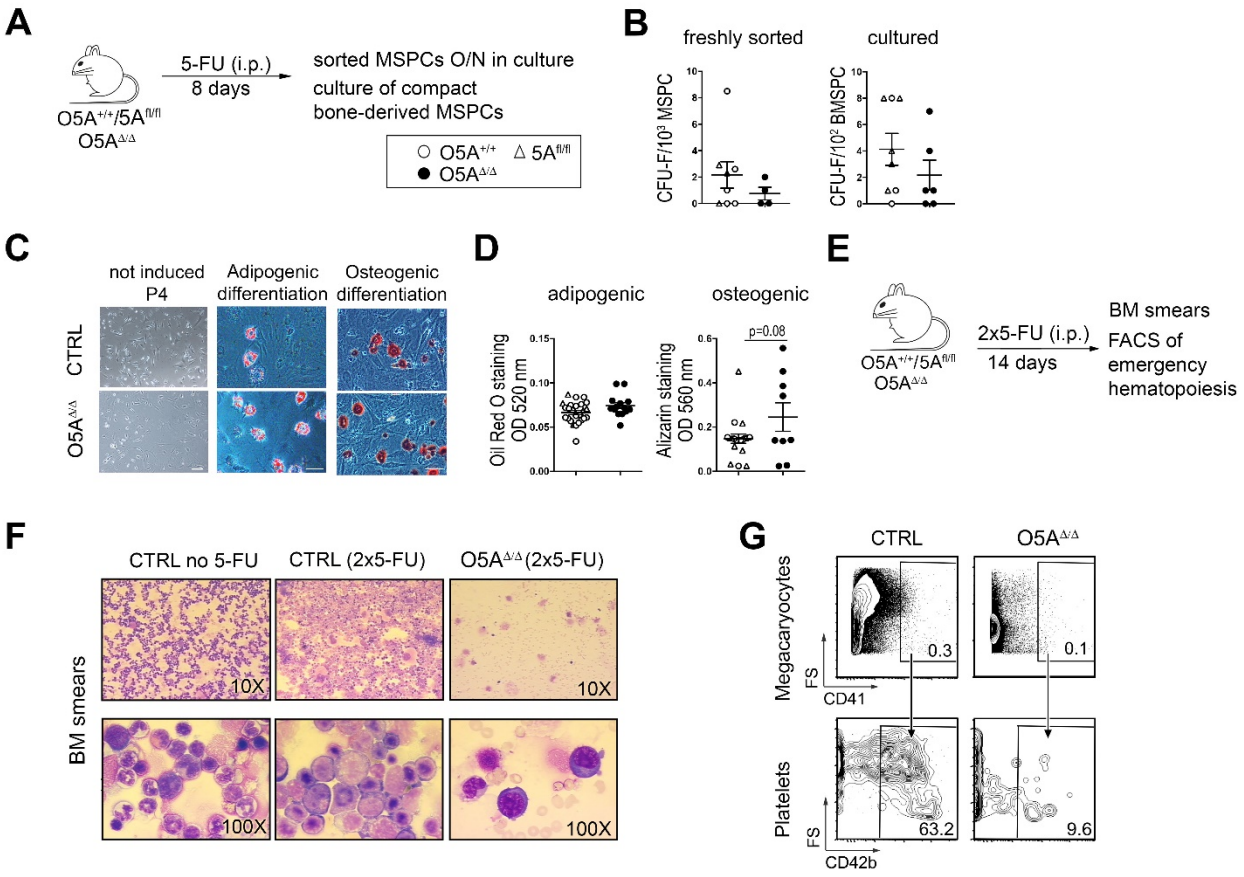

Figure S4. Niche analysis of 5-FU-treated O5A$^{\Delta/\Delta}$ mice. Related to Figure 1. A, *Experimental design for intraperitoneal (i.p.) injection of 5-FU in mice with the following genotypes: Control (CTRL): O5A$^{+/+}$, n=5, 5A$^{fl/fl}$, n=3 and O5A$^{\Delta/\Delta}$, n=4. Niche analysis 8 days after treatment.* ***B,*** *Counted CFU-F numbers of freshly sorted (TER119/CD45)$^{-}$ CD31^{-} CD51^{+} Alcam^{med} SCA-1^{+} immature MSPCs (P0/left) and compact bone-derived cultured MSPCs (p4/right).* ***C,*** *Representative microscope pictures of MSPCs (p4) in culture (not induced, left panels), after induction of adipogenic differentiation (middle panels) or osteogenic differentiation (right panels).* ***D,*** *Graphs showing adipogenic potential (left) and osteogenic potential (right) of compact bone-derived cultured MSPCs (P4) of both genotypes.* ***Bone marrow failure of 5-FU-treated O5A$^{\Delta/\Delta}$ mice. Related to Figure 2. E,*** *Experimental design for analysis of mice after two consecutive 5-FU treatments (day 0 and 8). CTRL: O5A$^{+/+}$, n= 7, 5A$^{fl/fl}$, n=11 and O5A$^{\Delta/\Delta}$, n=11.* ***F,*** *Representative pictures from BM smears from untreated CTRL (no 5-FU), and serial 5-FU treated controls and O5A$^{\Delta/\Delta}$ mice stained with May Grünwald and Giemsa staining. The bone marrow of 5-FU-treated control mice is hypercellular and dominated by erythropoietic cells. Erythropoiesis and granulopoiesis are both left-shifted, with almost no maturing cells beyond the basophilic erythroblast and the myelocyte, respectively. Megakaryocytes are elevated. In contrast, O5A$^{\Delta/\Delta}$ BM is extremely hypocellular. Only a few cells from the granulopoietic or erythropoietic lineage are visible.* ***G,*** *Representative FACS plots of emergency hematopoiesis in BM cells. CD41^{+} CD42^{+} Megakaryocytes. Scale bars, 10µm * p-value < 0.05 (non-parametric Mann-Whitney test: B and D). Data are represented as mean ± SEM. The 5-FU analysis and the consecutive 5FU analysis represent two to three independent experiments. Symbol legend shown in Figure S4A.*

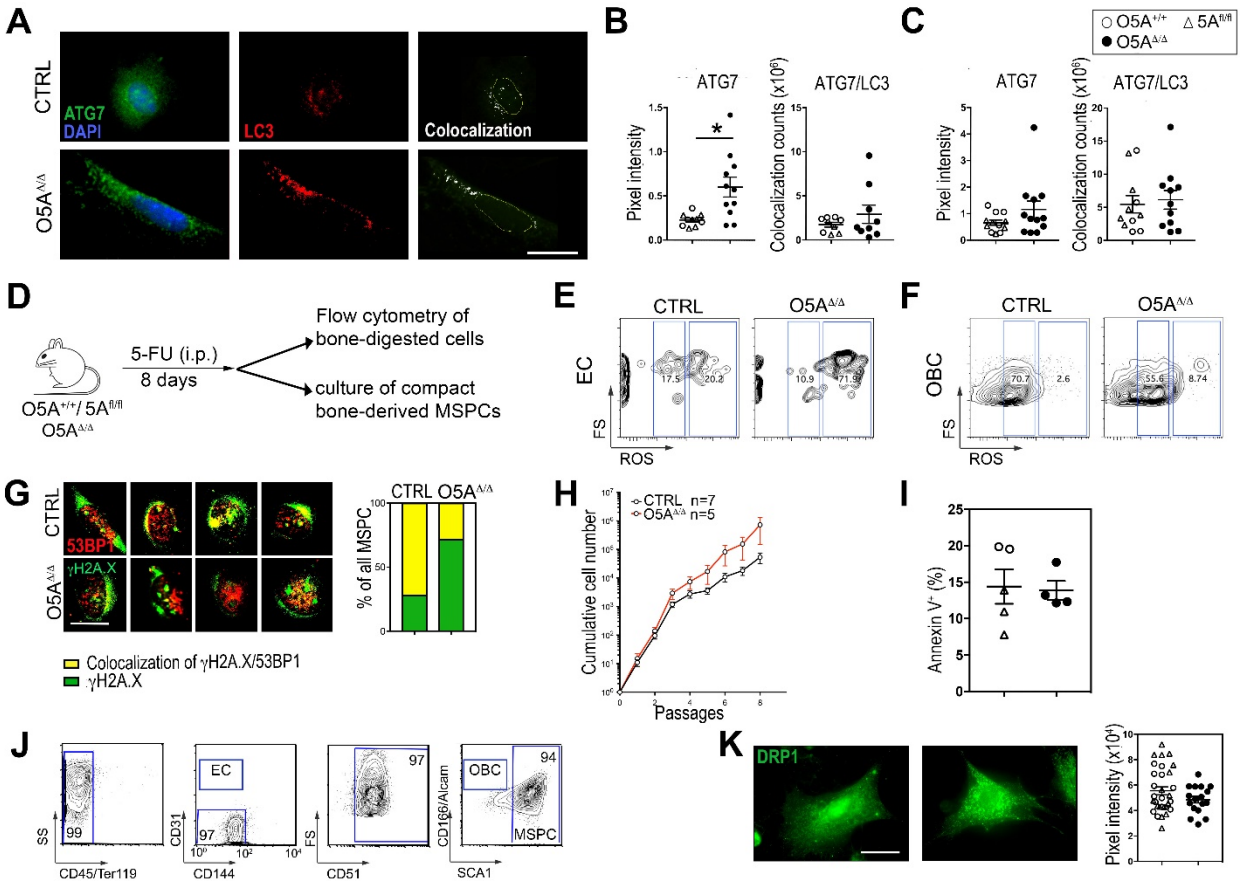

Figure S5. Autophagosome formation in mouse MSPCs of 5-FU-treated O5A$^{\Delta/\Delta}$ mice. Related to Figure 3. A, *Representative immunofluorescence pictures of ATG7 (green) and LC3 (red) and colocalization of ATG7/LC3 (white) in sorted MSPCs cultured O/N (p0).* ***B,*** *Graphs showing the pixel intensity of ATG7 (left) and colocalization of ATG7/LC3 (right) in sorted MSPCs cultured O/N (P0).* ***C,*** *Graphs showing the pixel intensity of ATG7 (left) and colocalization of ATG7/LC3 (right) in isolated and cultured compact bone-derived MSPCs (P4).* ***Characterization of compact bone-derived MSPCs (P4). Related to figure 4. D,*** *Experimental design as in previous Figures. Isolation and culture of compact bone-derived MSPCs. Control (CTRL): O5A$^{+/+}$, n=5, 5A$^{fl/fl}$, n=7 and O5A$^{\Delta/\Delta}$, n=10.* ***E, F,*** *Representative FACS plots of H_2DCFDA (ROS) detection in ECs (**E**) and OBCs (**F**) of CTRL (left) and O5A$^{\Delta/\Delta}$ (right) mice.* ***G,*** *Representative immunofluorescence pictures of yH2A.X (green) and 53BP1 (red) in compact bone-derived MSPCs (P4). Graph showing percentages of colocalized foci (yellow) and yH2A.X foci (green). The statistical analysis of colocalization shows a p-value of 0.09.* ***H,*** *Growth curve showing MSPC growth of CTRL (n=7) and O5A$^{\Delta/\Delta}$ (n=5) until passage 8.* ***I,*** *Graph showing percentages of annexinV^{+} (apoptotic and dead cells) of compact bone-derived MSPCs (P4) after trypsin digestion.* ***J,*** *Representative FACS plots of compact bone-derived MSPCs in culture (P4).* ***K,*** *Representative immunofluorescence pictures of DRP1 (green) in compact bone-derived MSPCs (P4) and graph showing the pixel intensity of protein content. Scale bars, 10µm. * p-value < 0.05 (Two-sided parametric student's t test: B, C, H, I, K). Data are represented as mean ± SEM. The analysis represents two to three independent experiments, except for the growth curve that represents one experiment with MSPCs from 4 donor mice grown in separate cultures. Symbol legend shown in Figure S5C.*

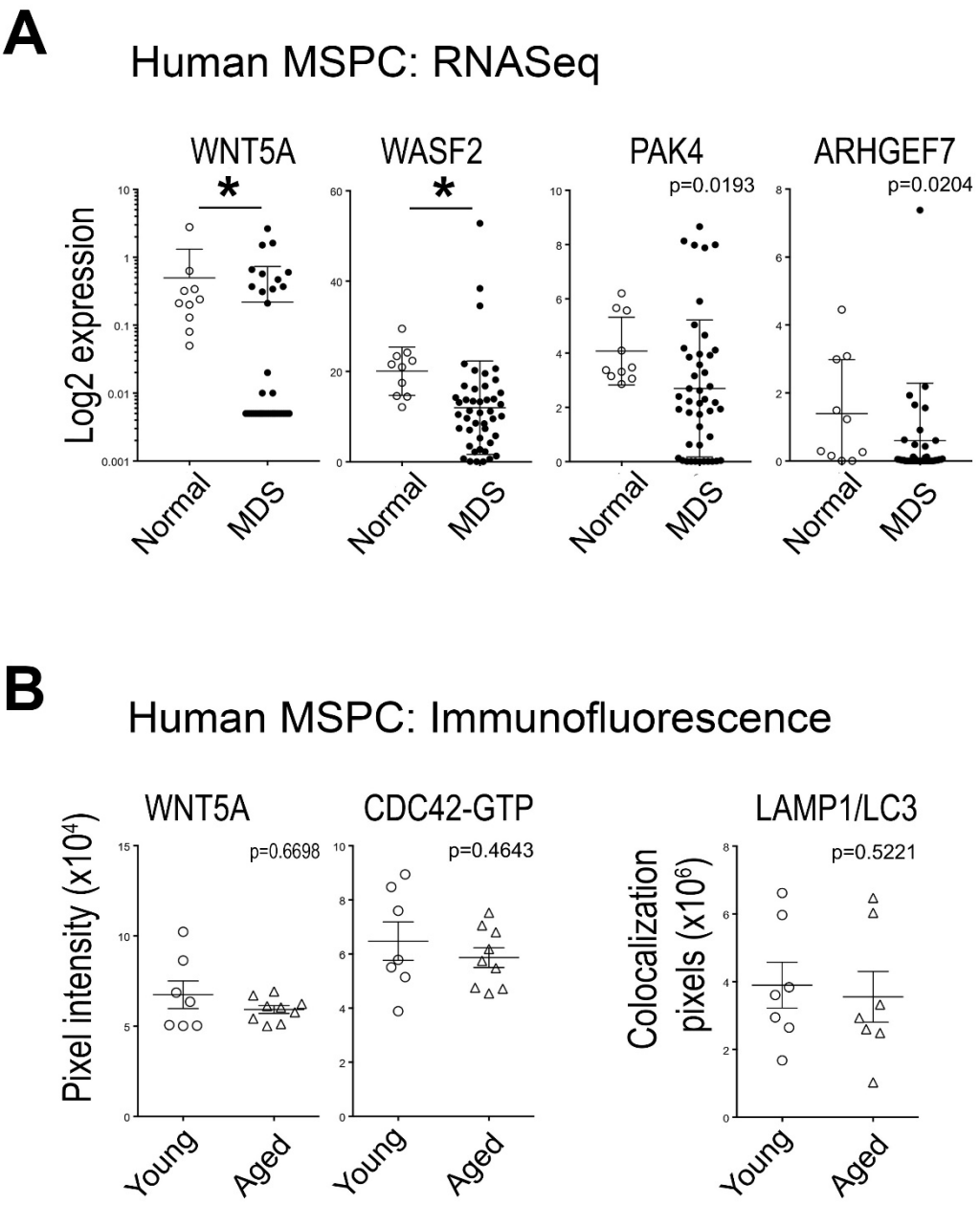

Figure S6. WNT5A-signaling in human MSPCs. Related to Figure 5. A, *RNASeq analysis of human MSPCs of MDS patients (n=45) compared to healthy individuals (n=10). Left graph shows WNT5A expression. No WNT5A expression in MDS patients: n=33. Normalized gene expression data were taken from the analysis of Zambetti et al.* [3]. ***B,*** *Pixel intensity of human MSPCs stained for WNT5A, CDC42-GTP and colocalization of LAMP1 and LC3 measured with ImageJ software. Each symbol represents the average of 30 cells. A: adjusted p-value < 0,0071 (Non parametric Mann-Whitney test), B: p-value < 0.05 (Non parametric Mann-Whitney test). Data are represented as mean ± SEM.*

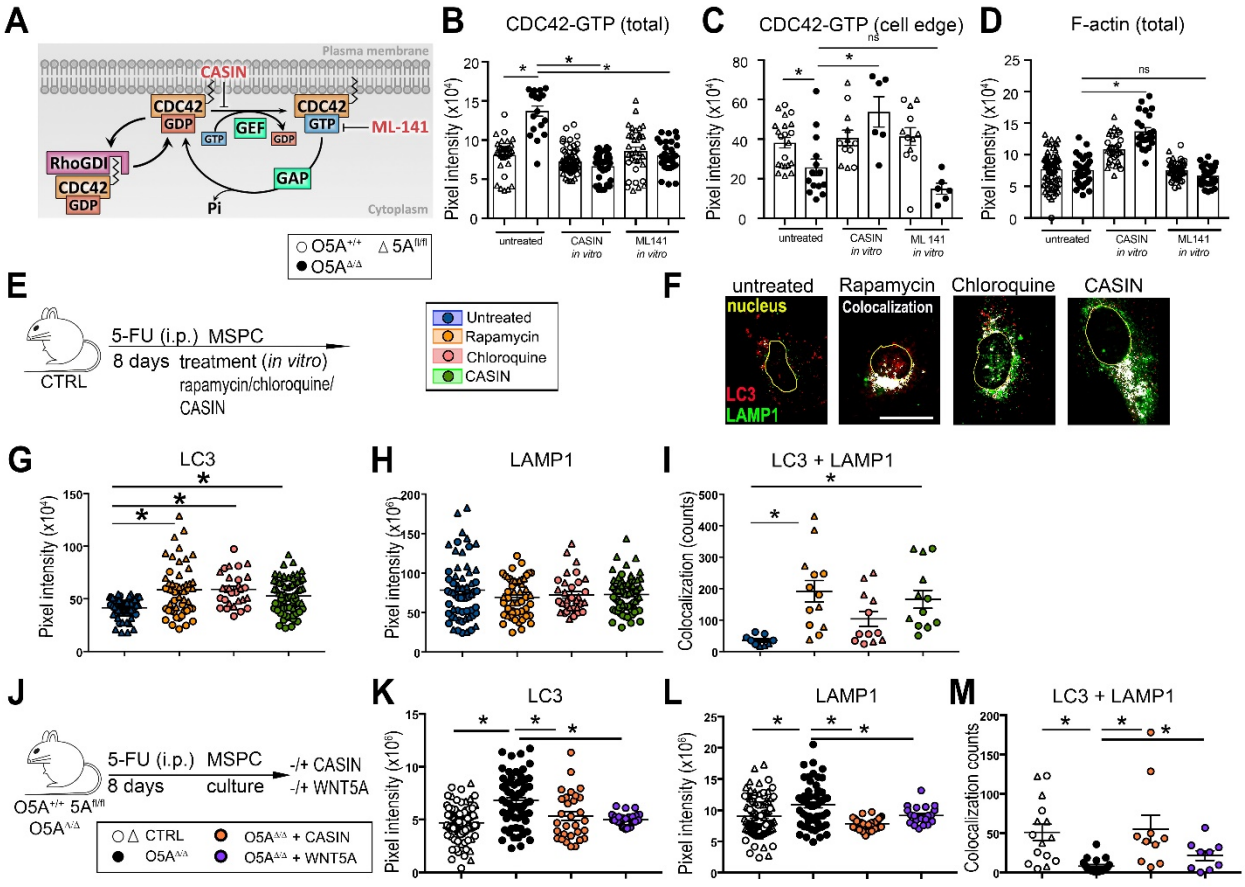

***Figure S7. Autophagic rescue in MSPCs of 5-FU-treated O5A$^{\Delta/\Delta}$ MSPCs. Related to Figure 6. A**, Inhibitors of CDC42, CASIN (CDC42-GDP/RhoGDI inhibitor) and ML141 (competitive CDC42-GTP inhibitor) and possible mechanisms (modified from [4]). **B, C** and **D,** In vitro treatment of MSPCs cultured from compact bones of 5-FU-treated mice with different genotypes. MSPCs were treated with CASIN (5μM) or ML141 (5μM) for 1 h in vitro, washed and stained for either an antibody against CDC42-GTP (**B, C**) or F-actin (Phalloidin, **D**). Fluorescent intensity staining (either total or at the cell edge) was assessed using ImageJ software. One representative experiment of three experiments is shown. **E,** Experimental design of MSPC culture from 5-FU-treated Control (CTRL) mice. In vitro treatment with rapamycin, chloroquine, or CASIN. **F,** Fluorescent microscopy images of LC3 (red) and LAMP1 (green). Colocalization shown in white measured by ImageJ software (plugin colocalization). **G, H, I,** Graphs showing colocalization counts (**I**) and pixel intensity of LAMP1 (**H**) and LC3 (**G**) measured by ImageJ software. **J,** Experimental design of MSPC culture from 5-FU-treated CTRL and O5A$^{\Delta/\Delta}$ mice. In vitro treatment with CASIN or rWNT5A. **K, L, M,** Graphs showing colocalization counts (**M**) and pixel intensity of LAMP1 (**L**) and LC3 (**K**) measured by ImageJ software. Scale bars, 10μm. * p-value < 0.05 (Non parametric Mann-Whitney test: B-D, G-I, K-M). Data are represented as mean ± SEM. Symbol legends shown in Figure S7A, S7E and S7J.*

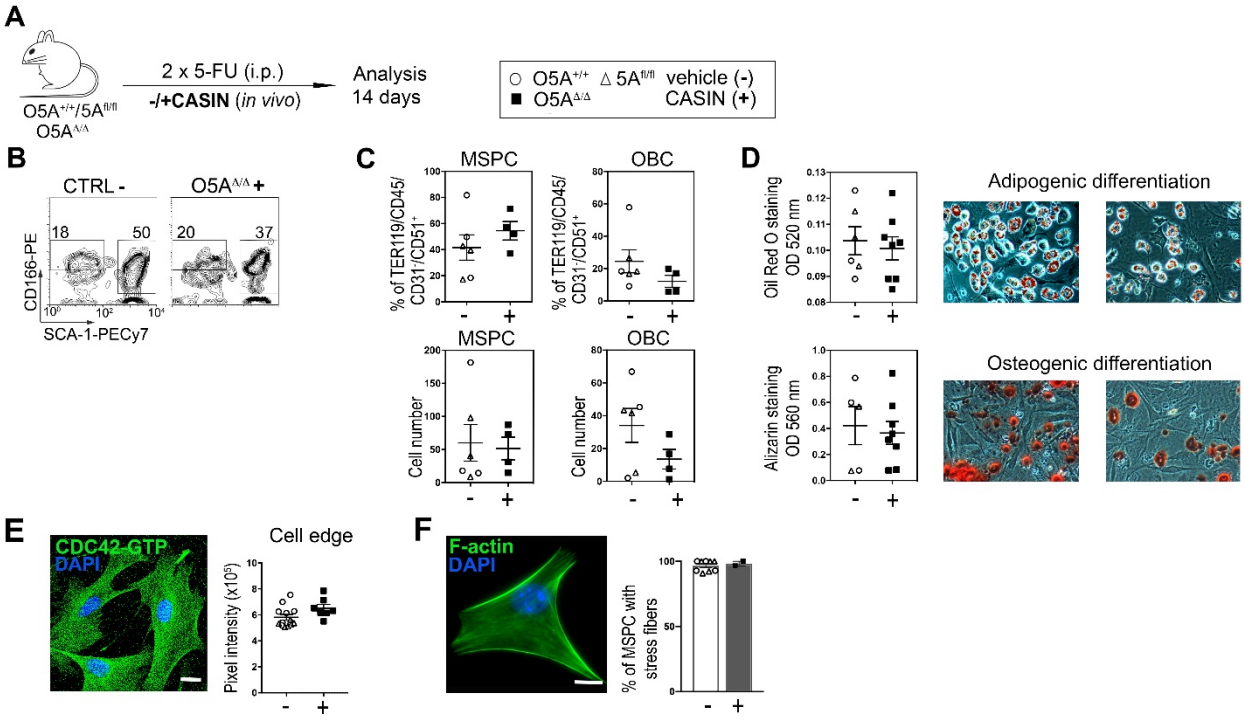

Figure S8. CDC42-GTP inhibition rescues hematopoiesis and niche remodeling. Related to Figure 6. A, *Experimental design for serial intraperitoneal (i.p.) injection (d0 and d8) of 5-FU and additional serial inhibitor CASIN (+) injection or vehicle (PBS + 15% ethanol (-)) (d5,6,7,8) in mice with the following genotypes: Control (CTRL): O5A$^{+/+}$, n=6, 5A$^{fl/fl}$, n=7 and O5A$^{\Delta/\Delta}$, n=7. Hematopoiesis and niche analysis 14 days after first 5-FU injection (d14).* ***B,*** *Representative FACS plots for OBCs (CD31$^-$ SCA-1$^-$ Alcam$^+$) and MSPCs (CD31$^-$ SCA-1$^+$ Alcam$^{-/low}$).* ***C,*** *Graphs showing the percentages and absolute numbers of MSPCs and OBCs.* ***D,*** *Graphs showing the adipogenic (upper panel) and osteogenic (lower panel) differentiation potential of cultured compact bone-derived MSPCs (P4). Representative pictures of oil red staining (upper panel) and alizarin red staining (lower panel).* ***E,*** *Representative fluorescent microscopy image of CDC42-GTP (green) and DAPI (blue) staining in MSPCs from O5A$^{\Delta/\Delta}$ CASIN treated (+) mice. Graph showing the pixel intensity of CDC42-GTP at the cell edge.* ***F****, Representative fluorescent microscopy image of F-actin (green) and DAPI (blue) staining in MSPCs from O5A$^{\Delta/\Delta}$ CASIN treated (+) mice. Graph showing percentage of MSPCs with stress fibers. Scale bars, 10µm * p-value < 0.05 (Non parametric Mann-Whitney test: C-F). Data are represented as mean ± SEM. The analysis represents two independent experiments. Symbol legend shown in Figure S8A.*

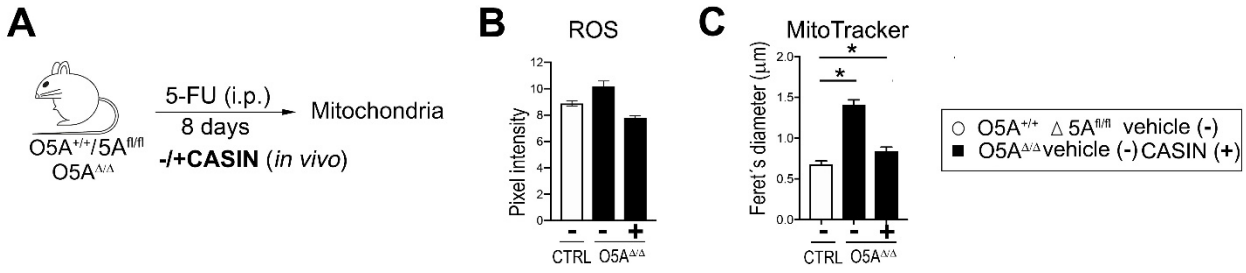

Figure S9. Mitochondria after in vivo 5-FU and CASIN treatment. Related to Figure 7. A, *Experimental design for intraperitoneal (i.p.) injection of 5-FU in mice with the following genotypes: Control (CTRL): O5A$^{+/+}$, n=10, 5A$^{fl/fl}$, n=10 and O5A$^{\Delta/\Delta}$, n=9. Additional in vivo i.p. injection of CDC42-GTP inhibitor CASIN (+) or vehicle (PBS + 15% ethanol (-)) at day 5-8 (d5,6,7,8). Analysis of mitochondrial metabolism in cultured MSPCs.* ***B,*** *Graph showing the pixel intensity of H_2DCFDA (ROS) in MSPCs with inhibitor treatment compared to vehicle treatment.* ***C,*** *Graph showing the results of MitoTracker Red staining designated as feret's diameter and measured by ImageJ software. *p-value < 0.05 (Two-sided parametric student's t test: B and C). Data are represented as mean ± SEM. The analysis represents two independent experiments. Symbol legend shown in Figure S9C.*

Supplementary Table 1

Experimental Models: Organisms/Strains		
Mouse: Osx-Cre: $O5A^{+/+}$	Jackson Labs	MGI: 006361
Mouse: $Wnt5a^{fl/fl}$: $5A^{fl/fl}$	Miyoshi et al., 2012	MGI: 5440733
Mouse: C57BL/6.J $Wnt5a^{fl/+}$	ZPF, MRI	MGI: N/A
Mouse: C57BL/6.J $Wnt5a^{\Delta/\Delta}$: $O5A^{\Delta/\Delta}$	ZPF, MRI	MGI: N/A
Mouse: 129S2: 129S2/SvPasCrl	Jackson Labs	MGI: 3587894
Mouse: Ly5.1: B6.SJL-Ptprca.Pep3b/BoyJ: B6 Cd45.1	Jackson Labs	MGI: 2164701
Oligonucleotides used for genotyping		
Wnt5A_Cond_F: TCTCGGAAGGTACTGCTATCTCCTACC	Miyoshi et al., 2012	N/A
Wnt5A_Cond_R: GGCTCCCTCAGTCAGTGTTTTCAT	Miyoshi et al., 2012	N/A
Wnt5A_Neo_F: GACTCAACAGCATTGAGACATGTTTGT	Miyoshi et al., 2012	N/A
OsterixCreTransgene_F: GAGAATAGGAACTTCGGAATAGTAAC	https://www.jax.org/strain/006361	N/A
OsterixCreTransgene_R: CCCTGGAAGTGACTAGCATTG	https://www.jax.org/strain/006361	N/A
OsterixCreInternControl_F: AGAGAGCTCCCCTCAATTATGT	https://www.jax.org/strain/006361	N/A
OsterixCreInternControl_R: AGCCACTTCTAGCACAAAGAACT	https://www.jax.org/strain/006361	N/A
Mouse: B6.SJL-Ptprca.Pep3b/BoyJ: B6 Cd45.1	Jackson Labs	MGI: 2164701

Supplementary Table 2:

attached file: Blood2021-011775 healthy donor and patient characteristics

Supplementary Table 3:

Antibodies used in this study		
CD45 Monoclonal Antibody (30-F11), FITC	eBioscience	Cat#11-0451-82; PRID: AB_465050
CD45 Monoclonal Antibody (30-F11), PE	eBioscience	Cat#12-0451-82; RRID: AB_465668
CD45 Monoclonal Antibody (30-F11), PE-Cyanine5.5	eBioscience	Cat#35-0451-82; RRID: AB_469718
CD45 Monoclonal Antibody (30-F11), PE-Cyanine7	eBioscience	Cat#25-0451-82; RRID: AB_2734986
CD45 Monoclonal Antibody (30-F11), APC	eBioscience	Cat#17-0451-82; RRID: AB_469392
CD45 Monoclonal Antibody (30-F11), APC-eFluor 780	eBioscience	Cat#47-0451-82; RRID: AB_1548781
CD45 Monoclonal Antibody (30-F11), Pacific Blue	Invitrogen	Cat#MCD4528; RRID: AB_10373710
CD3e Monoclonal Antibody (145-2C11), PE-Cyanine5.5	Invitrogen, eBioscience	Cat#35-0031-82; RRID: AB_11219266
TER-119 Monoclonal Antibody (TER119), PE	Invitrogen	Cat#MA5-17824; RRID: AB_2539207
CD45R (B220) Monoclonal Antibody (RA3-6B2), PE-Cyanine7	Invitrogen	Cat#25-0452-81; RRID: AB_469627
Ly-6G/Ly-6C Monoclonal Antibody (RB6-8C5), Pacific Blue	Invitrogen	Cat#RM3028; RRID: AB_10376182
CD11b Monoclonal Antibody (M1/70), APC-Cyanine7	Invitrogen	Cat#A15390; RRID: AB_2534404

CD45.1 Monoclonal Antibody (A20), FITC	Invitrogen, eBioscience	Cat#11-0453-82; RRID: AB_465058
CD45.2 Monoclonal Antibody (104), PE	Invitrogen, eBioscience	Cat#12-0454-81; RRID: AB_465678
CD45.2 Monoclonal Antibody (104), eFluor 450	Invitrogen, eBioscience	Cat#48-0454-82; RRID: AB_11042125
CD117 (c-Kit) Monoclonal Antibody (2B8), PE	Invitrogen, eBioscience	Cat#12-1171-82; RRID: AB_465813
CD34 Monoclonal Antibody (RAM34), FITC	Invitrogen, eBioscience	Cat#11-0341-81; RRID: AB_465021
CD34 Monoclonal Antibody (RAM34), eFluor 450	Invitrogen, eBioscience	Cat#48-0341-82; RRID: AB_2043837
CD150 Monoclonal Antibody (9D1), APC	Invitrogen, eBioscience	Cat#17-1501-63; RRID: AB_469440
Ly-6A/E (Sca-1) Monoclonal Antibody (D7), PE-Cyanine7	Invitrogen, eBioscience	Cat#25-5981-81; RRID: AB_469669
c-Kit Monoclonal Antibody (2B8), APC-Cyanine7	Invitrogen	Cat#A15423; RRID: AB_2534436
CD150 Monoclonal Antibody (9D1), PE	Invitrogen, eBioscience	Cat#12-1501-82; RRID: AB_465873
TER-119 Monoclonal Antibody (Ter119), PE-Cy5.5	Invitrogen, eBioscience	Cat#35-5921-82; PRID: AB_469738
CD31 (PECAM-1) Monoclonal Antibody (390), APC	Invitrogen, eBioscience	Cat#17-0311-82; RRID: AB_657735
CD144 (VE-cadherin) Monoclonal Antibody (eBioBV13), PB	Invitrogen, eBioscience	Cat#14-1441-82; PRID: AB_842767
CD166 (ALCAM) Monoclonal Antibody (eBioALC48), PE	Invitrogen, eBioscience	Cat#12-1661-81; RRID: AB_823125
TER-119 Monoclonal Antibody (TER119), Biotin	Invitrogen	Cat#MA5-17819; RRID: AB_2539203

CD51 (Integrin alpha V) Monoclonal Antibody (RMV-7), Biotin	Invitrogen, eBioscience	Cat#13-0512-85; RRID: AB_466477
CD41 Monoclonal Antibody (MWReg30), Biotin	Invitrogen	Cat#MA1-82655; RRID: AB_928291
CD48 Monoclonal Antibody (HM48-1), Biotin	Invitrogen, eBioscience	Cat#13-0481-82; RRID: AB_466470
CD11b Monoclonal Antibody (M1/70), Biotin	Invitrogen, eBioscience	Cat#13-0112-85; RRID: AB_466359
CD5 Monoclonal Antibody (53-7.3), Biotin	Invitrogen, eBioscience	Cat#13-0051-81; RRID: AB_466338
CD8a Monoclonal Antibody (53-6.7), Biotin	Invitrogen, eBioscience	Cat#13-0081-82; RRID: AB_466346
CD45R (B220) Monoclonal Antibody (RA3-6B2), Biotin	Invitrogen, eBioscience	Cat#13-0452-82; RRID: AB_466449
Ly-6G/Ly-6C Monoclonal Antibody (RB6-8C5), Biotin	Invitrogen, eBioscience	Cat#13-5931-86; RRID: AB_466802
Mouse Hematopoietic Lineage Biotin Panel	Invitrogen, eBioscience	Cat#88-7774-75; RRID: AB_476399
Streptavidin eFluor™ 450 Conjugate	eBioscience	Cat#48-4317-82; RRID: AB_10359737
Streptavidin, APC-Alexa Fluor™ 750	Invitrogen	Cat#SA1027; RRID: AB_2716627
Anti-mouse CD150 (SLAM) Antibody (TC15-12F12.2), PE	BioLegend	Cat#115904; RRID: AB_313683
Goat anti Mouse/Rat FABP4/A-FABP Antibody	R&D Systems	Cat#AF1443-SP; RRID: AB_2102444
Alexa Fluor® 647 AffiniPure Donkey Anti-Goat IgG (H+L)	Jackson ImmunoResearch	Cat#705-605-003; RRID: AB_2340436

Anti-phospho-Histone H2A.X (Ser139) Antibody (JBW301); mouse	Sigma-Aldrich	Cat#05-636; PRID: AB_309864
53BP1 Antibody, rabbit	Novus Biologicals	Cat#NB100-304SS; PRID: AB_920462
LAMP-1 Antikörper (1D4B); mouse	Santa Cruz	Cat#sc-19992; PRID: AB_2134495
LC3B Antibody; rabbit	Cell Signaling Technologies	Cat#2775; PRID: AB_915950
Phalloidin-iFluor 488 Reagent; conjugated iFluor 488	abcam	Cat#ab176753; PRID: N/A
Atg7 (D12B11) mAb; rabbit	Cell Signaling Technologies	Cat#8558; PRID: AB_10831194
Anti-Drp1 Clone 22/Drp1 (RUO); mouse	BDBiosciences	Cat#611738; PRID: AB_399214
Wnt-5a Antibody; goat	R&D Systems	Cat#AF645; PRID: AB_2288488
Active Cdc42-GTP; mouse	NewEast Bioscience	Cat#26905; PRID: AB_1961759
Recombinant Anti-TOMM20 antibody [EPR15581-54] - Mitochondrial Marker (Alexa Fluor® 555); mouse	abcam	Cat#ab221292; PRID: N/A
Human/Mouse/Rat p62/SQSTM1 Antibody; mouse	R&D Systems	Cat#MAB8028; PRID: N/A
CD41 Monoclonal Antibody (eBioMWReg30) eFluor 450	eBioscience	Cat#48-0411-82 PRID: AB_1582238
CD42b Monoclonal Antibody (HIP1), APC	eBioscience	Cat#17-0429-42 PRID: AB_2573146
Human Wnt-5a Antibody; rat	R&D Systems	Cat#MAB645-SP
Annexin V, FITC conjugate	eBioscience	Cat#A13199); PRID: N/A

MitoTracker™ Red CMXRos	Life Technologies	Cat#M7512
CM-H2DCFDA (General Oxidative Stress Indicator)	Life Technologies	Cat#C6827
CYTO-ID® Autophagy detection kit	Enzo Life Sciences	Cat#ENZ-51031-0050
Rabbit anti-Goat IgG (H+L) Cross-Adsorbed Secondary Antibody, Alexa Fluor 488	eBioscience	Cat#A-11078; PRID: AB_2534122
Donkey anti-Goat IgG (H+L) Cross-Adsorbed Secondary Antibody, Alexa Fluor 594	Invitrogen	Cat#A-11058; PRID: AB_2534105
Goat anti-Mouse IgG (H+L) Cross-Adsorbed Secondary Antibody, Alexa Fluor 488	Invitrogen	Cat#A-11001; PRID: AB_2534069
Goat anti-Rabbit IgG (H+L) Cross-Adsorbed Secondary Antibody, Alexa Fluor 488	Invitrogen	Cat#A-11008; RRID: AB_143165
Goat anti-Mouse IgG (H+L) Cross-Adsorbed Secondary Antibody, Alexa Fluor 594	Invitrogen	Cat#A-11005; RRID: AB_2534073
Donkey Anti-Goat IgG AffiniPure (H+L), Alexa Fluor® 647	Jackson ImmunoResearch	Cat#705-605-003; PRID: AB_2340436
Goat anti-rat IgG (H+L) Cross-Adsorbed Secondary Antibody, Alexa Fluor 488	Invitrogen	Cat#A-11006; RRID: AB_2534074

Supplementary Table 4

Software and Algorithms		
ImageJ Software	ImageJ NIH	https://imagej.nih.gov/ij/
Software Version Summit 4.4	Beckman Coulter	https://www.bioz.com/result/summit%20software/product/Beckman%20Coulter
FACS Diva Software v8.0	BD Biosciences	https://www.bdbiosciences.com/en-us/instruments/research-instruments/research-software/flow-cytometry-acquisition/facsdiva-software
FlowJo 8.8.6	BD Biosciences	https://www.flowjo.com

References to online supplement

1. Oostendorp RA, Medvinsky AJ, Kusadasi N, et al. Embryonal subregion-derived stromal cell lines from novel temperature-sensitive SV40 T antigen transgenic mice support hematopoiesis. *J Cell Sci*. 2002;115(Pt 10):2099-2108.
2. Liu W, Du W, Shang X, et al. Rational identification of a Cdc42 inhibitor presents a new regimen for long-term hematopoietic stem cell mobilization. *Leukemia*. 2019;33(3):749-761.
3. Zambetti NA, Ping Z, Chen S, et al. Mesenchymal Inflammation Drives Genotoxic Stress in Hematopoietic Stem Cells and Predicts Disease Evolution in Human Pre-leukemia. *Cell Stem Cell*. 2016;19(5):613-627.
4. Garcia-Mata R, Boulter E, Burridge K. The 'invisible hand': regulation of RHO GTPases by RHOGDIs. *Nat Rev Mol Cell Biol*. 2011;12(8):493-504.